Fluid and kinetic modeling of runaway electron generation from tritium beta decay and Compton scattering

I. Ekmark[1], M. Hoppe[2], T. Fülöp[1], R.A. Tinguely[3], R. Sweeney[4], P. Jansson[5], L. Antonsson[1], O. Vallhagen[1] and I. Pusztai[1]

[1]*Department of Physics, Chalmers University of Technology, Göteborg, Sweden.*
[2] *Department of Electrical Engineering, KTH Royal Inst. Technology, Stockholm, Sweden.*
[3]*Plasma Science and Fusion Center, Massachusetts Inst. Technology, Cambridge, MA, USA.*
[4]*Commonwealth Fusion Systems, Devens, MA, USA.*
[5]*Department of Computer Science and Engineering, Chalmers Univ. Technology, Göteborg, Sweden.*

Runaway electrons (REs) can be generated during tokamak disruptions and pose a critical challenge for future tokamaks. Accurate modelling of the primary generation mechanisms is crucial, due to the sensitivity of avalanche multiplication to the initial seed of REs. For this reason, we derive kinetic sources of energetic electrons from tritium beta decay and Compton scattering [1]. These kinetic models are then compared to well established fluid models for RE generation [2] through simulations of a SPARC primary reference discharge [3] scenario where the seed generation is dominated by the activated RE generation mechanisms.

Tritium beta decay The kinetic source due to tritium beta decay can be derived using the energy spectrum for beta electrons [4] $f_\beta(W) \propto F(p,2)p\mathcal{W}(W_{\max}-W)^2$ for $W \leq W_{\max}$. Here $\mathcal{W} = m_{\mathrm{e}}c^2\gamma$ is the total electron energy, $W = m_{\mathrm{e}}c^2(\gamma-1)$ is the electron kinetic energy, $\gamma = \sqrt{p^2+1}$ is the Lorentz factor and p is the momentum normalized to $m_{\mathrm{e}}c$. Since the maximum electron kinetic energy $W_{\max} = 18.6\,\mathrm{keV} \ll m_{\mathrm{e}}c^2 = 511\,\mathrm{keV}$, we may take the non-relativistic limit of the Fermi function [5], $F(p,Z_{\mathrm{f}}) = 2\pi\alpha Z_{\mathrm{f}}/\left[\beta\left(1-\exp(-2\pi\alpha Z_{\mathrm{f}}/\beta)\right)\right]$, with the normalized speed $\beta = p/\gamma$, the charge of the final state nucleus $Z_{\mathrm{f}} = 2$, and the fine structure constant $\alpha \approx 1/137$. The emission angle of electrons during the decay is assumed to be random and uniformly distributed. Therefore, the source can be assumed to be isotropic in pitch angle, and we may write

$$4\pi p^2 \mathrm{d}p \left(\frac{\mathrm{d}f}{\mathrm{d}t}\right)_{\mathrm{T}} = \mathrm{d}W f_\beta(W) \implies \left(\frac{\mathrm{d}f}{\mathrm{d}t}\right)_{\mathrm{T}} = \frac{m_{\mathrm{e}}c^2\beta}{4\pi p^2} f_\beta(W) \propto \frac{1}{p^2}\frac{p\gamma(\gamma_{\max}-\gamma)^2}{1-\exp[-4\pi\alpha/\beta]}. \quad (1)$$

This source integrated over the entire momentum space should yield the tritium decay rate, i.e.

$$\left(\frac{\mathrm{d}f}{\mathrm{d}t}\right)_{\mathrm{T}} = \frac{1}{C}\frac{\ln 2}{4\pi}\frac{n_{\mathrm{T}}}{\tau_{\mathrm{T}}}\frac{1}{p^2}\frac{p\gamma\left(\gamma_{\max}-\gamma\right)^2}{1-\exp(-4\pi\alpha/\beta)},\ C = \int_0^{p_{\max}} \frac{1}{p^2}\frac{p\gamma\left(\gamma_{\max}-\gamma\right)^2}{1-\exp(-4\pi\alpha/\beta)} p^2 \mathrm{d}p, \quad (2)$$

where the half-life for tritium $\tau_{\mathrm{T}} \approx 12$ years and $p_{\max}$ is the momentum corresponding to $W_{\max}$.

Compton scattering The Compton scattering process is described by the Klein-Nishina differential cross-section

$$\frac{\mathrm{d}\sigma}{\mathrm{d}\Omega} = \frac{r_{\mathrm{e}}^2}{2}\frac{W_\gamma'^2}{W_\gamma^2}\left[\frac{W_\gamma}{W_\gamma'} + \frac{W_\gamma'}{W_\gamma} - \sin^2(\theta)\right], \quad (3)$$

where r_{e} is the classical electron radius. Using the kinematic relation between the photon energy W_γ, the electron kinetic energy W and deflection angle θ of the scattered photon, we can write

$$\cos\theta = 1 - m_{\mathrm{e}}c^2 W/\left(W_\gamma W_\gamma'\right), \quad (4)$$

where $W_\gamma' = W_\gamma - W$ is the scattered photon energy. This source can also be assumed to be

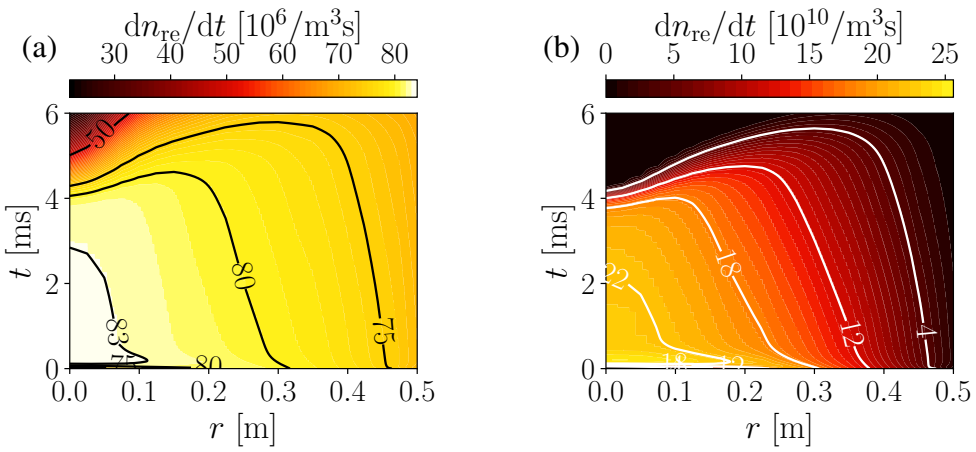

Figure 1: The kinetic sources from (a) tritium beta decay and (b) Compton scattering, integrated from p_c according to equation (7), are plotted as colored (and filled) contours, as functions of radius and time. On top of these are the fluid generation rates plotted as contour lines.

isotropic, since gamma photons will be emitted from the walls and enter the plasma from all sides in a nearly isotropic manner. Thus, in a plasma with total electron density $n_{\mathrm{e,tot}}$, including both free and bound electrons, we can write

$$4\pi p^2 \mathrm{d}p \left(\frac{\mathrm{d}f}{\mathrm{d}t}\right)_{\mathrm{C}} = n_{\mathrm{e,tot}} \int_{W_{\gamma 0}}^{\infty} \mathrm{d}W_\gamma \left[\Gamma_\gamma(W_\gamma)\left(2\pi \sin\theta \frac{\mathrm{d}\sigma}{\mathrm{d}\Omega}\right)\mathrm{d}\theta(W, W_\gamma)\right], \tag{5}$$

where Γ_γ is the photon energy spectrum and the lower integration limit can be derived from (4) as $W_{\gamma 0} = (p+\gamma-1)/2$. Thus the energetic electron source rate from Compton scattering

$$\left(\frac{\mathrm{d}f}{\mathrm{d}t}\right)_{\mathrm{C}} = \frac{n_{\mathrm{e,tot}}}{2}\frac{1}{p^2}\int_{W_{\gamma 0}}^{\infty} \mathrm{d}W_\gamma \Gamma_\gamma(W_\gamma)\frac{\mathrm{d}\sigma}{\mathrm{d}\Omega}\frac{\beta}{\left(W_\gamma/m_\mathrm{e}c^2+1-\gamma\right)^2}, \tag{6}$$

where we have used $\mathrm{d}\theta/\mathrm{d}p = \beta/\left[\sin\theta\left(W_\gamma/m_\mathrm{e}c^2+1-\gamma\right)^2\right]$.

Both kinetic sources are consistent with the fluid sources presented in [2], since

$$\left(\frac{\mathrm{d}n_{\mathrm{re}}}{\mathrm{d}t}\right)_{\mathrm{T}} = \ln 2 \frac{n_{\mathrm{T}}}{\tau_{\mathrm{T}}}\int_{W_\mathrm{c}}^{W_{\max}} f_\beta(W)\mathrm{d}W = \int_{p>p_\mathrm{c}}^{p<p_{\max}} \mathrm{d}^3p \left(\frac{\mathrm{d}f}{\mathrm{d}t}\right)_{\mathrm{T}}, \tag{7a}$$

$$\left(\frac{\mathrm{d}n_{\mathrm{re}}}{\mathrm{d}t}\right)_{\mathrm{C}} = n_\mathrm{e}^{\mathrm{tot}}\int_{W_{\gamma 0}}^{\infty}\Gamma_\gamma(W_\gamma)\int_{\theta_\mathrm{c}}^{\pi}\frac{\mathrm{d}\sigma}{\mathrm{d}\Omega}\mathrm{d}\Omega\mathrm{d}W_\gamma = \int_{p>p_\mathrm{c}}\mathrm{d}^3p\left(\frac{\mathrm{d}f}{\mathrm{d}t}\right)_{\mathrm{C}}, \tag{7b}$$

where W_c is the energy and θ_c the deflection angle corresponding to the critical momentum p_c. This was also confirmed by running SPARC simulations with the kinetic and the fluid sources and comparing the generation above the critical momentum. As shown in figure 1, the integrated kinetic sources and the fluid rates agree well in both values and contour shapes.

Simulation setup To compare the derived kinetic activated sources with the fluid sources derived in [2], we have performed reduced kinetic simulations with the DREAM code [6]. We have considered three cases – a case without any generation from the activated sources, a case with the fluid activated sources and a case with the kinetic activated sources.

All simulations treat the hot electrons ($p \sim p_\mathrm{c}$) kinetically, while the cold bulk electrons ($p \ll p_\mathrm{c}$) and the REs ($p \gg p_\mathrm{c}$) are treated as fluids. Such division of the electrons into three

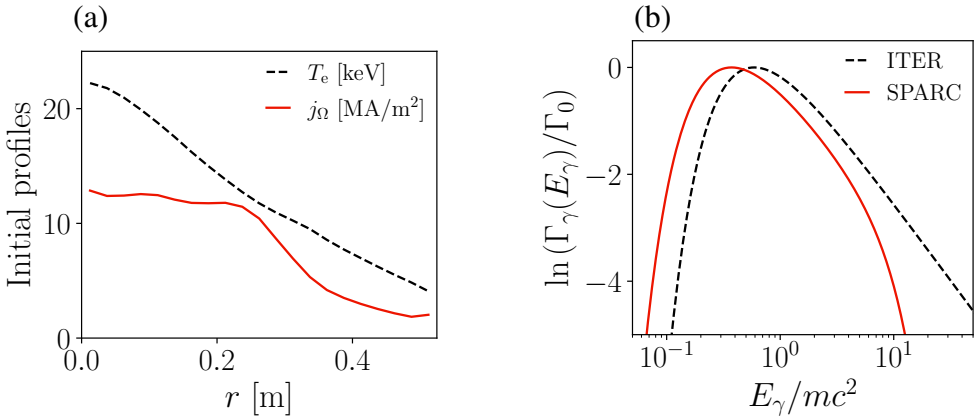

Figure 2: (a) Initial temperature and ohmic current density profiles, and (b) normalized photon energy spectrum for SPARC compared to ITER [2], used for the SPARC simulations.

populations which are modeled differently is especially practical for simulations including Massive Material Injection (MMI), where there is the hot initial plasma and cold injected material. The distribution function for the hot electrons is evolved using the pitch-angle averaged Fokker-Planck equation described in Appendix B.2 of [6], which assumes that the pitch angle scattering is the dominating effect. This is typically valid for electrons with $p \leq p_c$, meaning that such a model is suitable for studying the electrons involved in the seed generation.

We have simulated the SPARC primary reference discharge, which has an initial plasma current $I_p = 8.7\,\mathrm{MA}$, major radius $R_0 = 1.85\,\mathrm{m}$, minor radius $a = 0.57\,\mathrm{m}$ and on axis magnetic field $B_0 = 12.2\,\mathrm{T}$. The disruption was caused by MMI of deuterium, with density $n_D \sim 10^{22}\,\mathrm{m}^{-3}$, and neon, with density $n_{Ne} \sim 10^{20}\,\mathrm{m}^{-3}$, deposited instantly and uniformly. The densities were chosen such that the RE seed generation was dominated by the activated sources, which resulted in a low RE current relative to the expected unmitigated RE current of $\sim 5.5\,\mathrm{MA}$ [7]. The initial temperature and ohmic current profiles used for the simulations are shown in figure 2.a.

The energy spectrum $\Gamma_\gamma(W_\gamma) = \Gamma_{\mathrm{flux}} \exp[-\exp(-z) - z + 1] \,/ \int \exp[-\exp(-z) - z + 1]\,\mathrm{d}W_\gamma$ for the Compton photons, where $z = [\ln(W_\gamma/10^6) + C_1]/C2 + C_3(W_\gamma/10^6)^2$, is based on the one estimated for ITER in [2]. The C_3-term is added compared to the form in [2] to achieve a steeper decrease for higher photon energies, and the parameters C_1, C_2 and C_3 have been fitted to preliminary data obtained from MCNP simulations [8] – the photon energy spectrum used is plotted in figure 2.b together with the ITER spectrum [2]. Based on [8], the prompt emission photon flux for full fusion power in SPARC $\Gamma_{\mathrm{flux}} \sim 10^{18}/(\mathrm{m}^2\mathrm{s})$. We have assumed that the flux from the activated walls reduces to $\Gamma_{\mathrm{flux}} \sim 10^{15}/(\mathrm{m}^2\mathrm{s})$ when fusion power has ceased.

Results In the simulation without activated sources, negligible RE current is generated according to figure 3.a, indicating that any generation from other seed generation mechanisms is negligible for this SPARC scenario. The simulation with the fluid sources generates $1.08\,\mathrm{MA}$ RE current. With the kinetic sources we get a $1.35\,\mathrm{MA}$ RE current. Notably, these RE currents

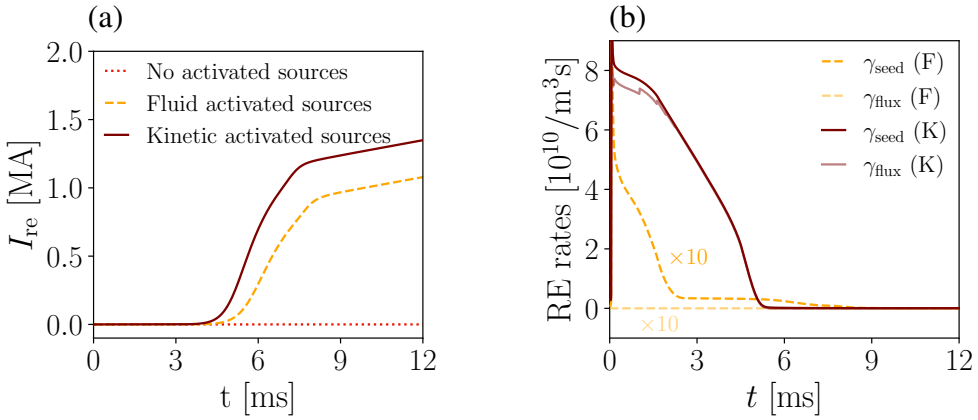

Figure 3: (a) RE current, and (b) total seed and momentum space flux RE generation at the core, for the simulations with the no (red in a), fluid (yellow) and kinetic (auburn) activated sources. Note that the fluid generation rates are multiplied by a factor of 10.

are much smaller than the expected unmitigated RE current in SPARC of $\sim 5.5\,\mathrm{MA}$ [7].

In figure 3.b we show the differences between the fluid and kinetic RE seed generation rates and the flux over the critical momentum boundary (i.e. p_{c}). Here, we define the total seed generation as $\gamma_{\mathrm{seed}} = \mathrm{d}n_{\mathrm{re}}/\mathrm{d}t - \gamma_{\mathrm{A}}$, where γ_{A} is the avalanche generation rate, and the generation from flux across p_{c} as $\gamma_{\mathrm{flux}} = \gamma_{\mathrm{seed}} - (\mathrm{d}n_{\mathrm{re}}/\mathrm{d}t)_{\mathrm{T}} - (\mathrm{d}n_{\mathrm{re}}/\mathrm{d}t)_{\mathrm{C}}$, where the two activated source terms for the kinetic sources are defined as in equation (7). With the kinetic sources, which add electrons to the distribution function for the hot electrons, the RE generation can be divided into two parts. Electrons appearing at $p > p_{\mathrm{c}}$ which will immediately run away, which is the generation defined by equation (7), and this generation is identical to the generation of the fluid sources. However, electrons with $p < p_{\mathrm{c}}$ will also be generated, and they can run away as part of the flux over the critical momentum boundary. As shown in figure 3.b, the generation from momentum space flux is negligible in the simulation with fluid sources, but is the dominating generation mechanism in the simulation with the kinetic sources. The additional generation from the activated sources due to momentum space dynamics – captured by the derived kinetic activated sources – can thus have a significant effect on the generated RE current.

Summary We derived kinetic sources of energetic electrons generated by tritium beta decay and Compton scattering and compared them to the corresponding fluid RE generation rates [2]. In the SPARC example considered, using kinetic (as opposed to fluid) sources yielded $25\,\%$ higher RE current. The reason for this is that energetic electrons generated by the kinetic sources with $p < p_{\mathrm{c}}$ can run away since collisions for these electrons are kinetically resolved.

[1] I. Ekmark et al., JPP, **90**, 905 900 306 (2024).
[2] J.R. Martín-Solís et al., NF, **57**, 066 025 (2017).
[3] A.J. Creely et al., JPP, **86**, 865 860 502 (2020).
[4] K.S. Krane, *Introductory Nuclear Physics*, (1988).
[5] E. Fermi, Zeitschrift f. Phys., **88**, 161–177 (1934).
[6] M. Hoppe et al., CPC, **268**, 108 098 (2021).
[7] R.A. Tinguely et al., NF, **61**, 124 003 (2021).
[8] H. Boyd (CFS), personal communication (2024).

This work has been carried out within the framework of the EUROfusion Consortium, funded by the European Union via the Euratom Research and Training Programme (Grant Agreement No 101052200 — EUROfusion). Views and opinions expressed are however those of the author(s) only and do not necessarily reflect those of the European Union or the European Commission. Neither the European Union nor the European Commission can be held responsible for them.

Supported in part by Commonwealth Fusion Systems.